Title

Precession modulation of the South Pacific westerly wind belt over the past million years.

Journal

Proceedings of the National Academy of Sciences of the United States of America, 116(47)

ISSN

0027-8424

Authors

Lamy, Frank
Chiang, John CH
Martínez-Méndez, Gema
et al.

Publication Date

2019-11-01

DOI

10.1073/pnas.1905847116

Peer reviewed

Precession modulation of the South Pacific westerly wind belt over the past million years

Frank Lamy[a,1], John C. H. Chiang[b], Gema Martínez-Méndez[a,c], Mieke Thierens[a], Helge W. Arz[d], Joyce Bosmans[e], Dierk Hebbeln[c], Fabrice Lambert[f], Lester Lembke-Jene[a], and Jan-Berend Stuut[g,h]

[a]Marine Geology Section, Alfred-Wegener-Institut Helmholtz-Zentrum für Polar- und Meeresforschung, 27570 Bremerhaven, Germany; [b]Department of Geography, University of California, Berkeley, CA 94720-4740; [c]Center for Marine Environmental Sciences, University of Bremen, 28334 Bremen, Germany; [d]Department of Marine Geology, Leibniz Institute for Baltic Sea Research, 18119 Rostock-Warnemünde, Germany; [e]Department of Physical Geography, Utrecht University, 3584 CB, Utrecht, The Netherlands; [f]Department of Physical Geography, Pontifical Catholic University of Chile, 7820436 Santiago, Chile; [g]Royal Netherlands Institute for Sea Research (NIOZ), Ocean Systems (TX), Utrecht University, 1790 AB, Den Burg, Texel, The Netherlands; and [h]Faculty of Science, Department of Earth Sciences, Vrije Universiteit Amsterdam, 1081 HV, Amsterdam, The Netherlands

Edited by James P. Kennett, University of California, Santa Barbara, CA, and approved October 6, 2019 (received for review April 5, 2019)

The southern westerly wind belt (SWW) interacts with the Antarctic Circumpolar Current and strongly impacts the Southern Ocean carbon budget, and Antarctic ice-sheet dynamics across glacial–interglacial cycles. We investigated precipitation-driven sediment input changes to the Southeast Pacific off the southern margin of the Atacama Desert over the past one million years, revealing strong precession (19/23-ka) cycles. Our simulations with 2 ocean–atmosphere general circulation models suggest that observed cyclic rainfall changes are linked to meridional shifts in water vapor transport from the tropical Pacific toward the southern Atacama Desert. These changes reflect a precessional modulation of the split in the austral winter South Pacific jet stream. For precession maxima, we infer significantly enhanced rainfall in the southern Atacama Desert due to a stronger South Pacific split jet with enhanced subtropical/subpolar jets, and a weaker midlatitude jet. Conversely, we derive dry conditions in northern Chile related to reduced subtropical/subpolar jets and an enhanced midlatitude jet for precession minima. The presence of precessional cycles in the Pacific SWW, and lack thereof in other basins, indicate that orbital-scale changes of the SWW were not zonally homogeneous across the Southern Hemisphere, in contrast to the hemispherewide shifts of the SWW suggested for glacial terminations. The strengthening of the jet is unique to the South Pacific realm and might have affected winter-controlled changes in the mixed layer depth, the formation of intermediate water, and the buildup of sea-ice around Antarctica, with implications for the global overturning circulation and the oceanic storage of atmospheric CO_2.

orbital cycles | southern westerly wind belt | quaternary | paleoclimate

The Southern Hemisphere westerly wind belt (SWW) plays an important role in mid- and high-latitude atmosphere–ocean dynamic. As such, variations in the high-altitude jet stream of the SWW are critical for communicating climate signals between low and high latitudes (1). Together with Southern Ocean buoyancy (2), the SWW represents the major forcing of the Antarctic Circumpolar Current (3). These atmosphere–ocean processes control the upwelling of carbon-rich deep-water masses in the Southern Ocean, thereby affecting atmospheric CO_2 changes over glacial cycles (4, 5) and the Holocene (6, 7). In addition, the strength of the midlatitude and subpolar westerlies affects warm Circumpolar Deep-Water incursions onto the West Antarctic continental shelf (8), impacting the stability of the West Antarctic Ice Sheet via submarine basal melting (9). In contrast to the Atlantic and Indian Ocean sectors, during austral winter, the Pacific SWW is characterized by a split of the high-altitude jet stream into strong subtropical and subpolar jets, and a weaker midlatitude jet (10–12). Variations in these jets affect the strength and latitudinal position of the South Pacific surface westerlies, altering the forcing on the wind-driven ocean circulation in the South Pacific.

Beyond the short instrumental record (13), proxy data-based reconstructions of the SWW traditionally focus on the Holocene (6, 7) and the Last Glacial Maximum (LGM) (14, 15). These studies indicate an overall northward shift and/or intensification of the SWW during the LGM and a similar trend from the Early to Late Holocene. At millennial timescales across the last glacial termination and during Marine Isotope Stage 3, it has been argued that the SWW plays a role in the interhemispheric transfer of climate signals between the North Atlantic region and the Southern Hemisphere mid- and high latitudes (4, 16–18). Most previous studies assume zonally symmetric shifts or intensity changes of the westerlies across the Southern Hemisphere at millennial and orbital timescales, but modern variability of the SWW at interannual to decadal timescales also exhibits pronounced zonally asymmetric changes (19, 20), such as modulation of the South Pacific Split Jet (11, 20) or SWW changes related to the El Niño-Southern Oscillation (21).

Evidence for changes in the SWW on orbital timescales and across multiple glacial–interglacial cycles is very limited (22–25). Here, we present an ∼950-ka-long marine sediment record, recovered

Significance

The southern westerly wind belt interacts with the Antarctic Circumpolar Current and strongly impacts the Southern Ocean carbon budget, and Antarctic ice-sheet dynamics across glacial–interglacial cycles. We investigated precipitation-driven sediment input changes to the Pacific off Chile over the past one million years, revealing strong precession (19/23-ka) cycles. Our model simulations indicate that the observed cycles are linked to meridional shifts in water vapor transport from the tropical Pacific toward Chile, ultimately forced by variations of the subtropical jet. The wintertime strengthening of the jet is unique to the South Pacific realm and affects winter-controlled atmosphere–ocean processes at mid- and high southern latitudes, with implications for the global overturning circulation and the oceanic storage of atmospheric CO_2.

Author contributions: F. Lamy, J.C.H.C., H.W.A., and D.H. designed research; F. Lamy, J.C.H.C., M.T., J.B., F. Lambert, and L.L.-J. performed research; F. Lamy, J.C.H.C., G.M.-M., M.T., H.W.A., J.B., F. Lambert, and J.-B.S. analyzed data; and F. Lamy, J.C.H.C., G.M.-M., H.W.A., J.B., and L.L.-J. wrote the paper.

The authors declare no competing interest.

This article is a PNAS Direct Submission.

Data deposition: The Geophysical Fluid Dynamics Laboratory data have been archived at University of California, Berkeley Dash, Dataset, https://datadryad.org/stash/dataset/doi:10.6078/D1DX1P. EC-Earth model output is available from Zenodo. http://doi.org/10.5281/zenodo.3268528. Paleoproxy data presented in this study are available in the Supporting Information and at PANGAEA, https://doi.org/10.1594/PANGAEA.907631.

[1]To whom correspondence may be addressed. Email: Frank.Lamy@awi.de.

This article contains supporting information online at www.pnas.org/lookup/suppl/doi:10.1073/pnas.1905847116/-/DCSupplemental.

First published November 4, 2019.

from the Chilean continental slope at 27.5°S off the southern Atacama Desert, documenting austral winter rain changes at the northernmost SWW in the Southeast Pacific. Our study provides evidence that the austral winter SWW varied zonally asymmetrically on precessional timescales with important implications for seasonal Southern Ocean atmosphere–ocean changes.

Winter Rain Changes in Northern Chile and the Strength of the Pacific Subropical Jet (STJ)

Sedimentological data are based on sediment core GeoB3375-1 (26), combined with a composite record from the Center for Marine Environmental Sciences (MARUM) deep-sea drill-rig (MeBo) site GeoB15016 (27) (*SI Appendix*, Fig. S1). The sites are located ~25–35 km WSW off the mouth of the Copiapó River. Sediments at both sites are mainly composed of siliciclastic material and biogenic carbonate ($CaCO_3$ contents range from ~5 to ~40%). Lithologically, the sediments are composed of homogeneous calcareous microfossil-bearing clayey silt with subtle color changes (*SI Appendix*). We use high-resolution records of logarithm-normalized changes in iron to calcium ratios [log (Fe/Ca) following (28)] to document variations in the amount of terrigenous sediments and grain-size analyses of the siliciclastic sediment fraction to infer changes in the mode of sediment input (Fig. 1 and *SI Appendix*, Fig. S2). Consistent with earlier observations [e.g., the ~120-ka record from core GeoB3375-1 (26, 29)], iron-rich sediments [higher log (Fe/Ca)] are finer grained and more poorly sorted, with lower carbonate percent throughout the ~950-ka record. Conversely, the siliciclastic fraction of more carbonate-rich sediments [lower log (Fe/Ca)] is coarser grained and better sorted.

Presently, the Chilean Norte Chico at the southern border region of the Atacama Desert is characterized by prevailing arid conditions and dry valleys with only sporadic water runoff and eolian sediment input to the ocean (30, 31) with mean grain-size and -sorting characteristics similar to those found in our sediment records. Sediments derived from volcanic source rocks in the Andes are mostly trapped in the alluvial basins east of the Coastal Range and do not reach the ocean (*SI Appendix*, Fig. S1). During more humid periods in the past, the dry valleys were activated and the supply of fluvially derived sediments to our coring sites was enhanced (26, 29). Therefore, the well-defined variations in sediment composition off northern Chile indicate changes in the relative contributions of fluvial [higher log (Fe/Ca), finer mean grain size, poorer sorted] and eolian [lower log (Fe/Ca), coarser mean grain size, better sorted] sediment supply. The only modern perennial river in the area is the Copiapó River (*SI Appendix*, Fig. S1), characterized by a primary discharge peak in summer and a secondary peak in winter (32, 33). The main peak is due to snow melt accumulated in the previous winter, while the winter peak is directly recording winter precipitation and/or lagged groundwater discharge originating from the summer snow melt (32, 33).

The log (Fe/Ca) record is characterized by pronounced orbital-scale variations in all Milankovitch orbital bands (Fig. 1*E*). The most striking feature is the strong spectral power in the precessional band (~19–23-ka cycles), consistent with earlier findings on core GeoB3375-1 (26, 29, 34). Our record extends this cyclicity back to ~950 ka BP, showing high cross-spectral coherency at both the 19- and 23-ka precessional bands (Fig. 1*E*). Average sedimentation rates of ~6 cm/ka and reliable age control, primarily based on benthic foraminiferal oxygen isotope ($\delta^{18}O$) stratigraphy (27) (Fig. 1*A* and *SI Appendix*, Fig. S3), enable us to resolve these precessional cycles. The phasing between log (Fe/Ca) and precession is constrained by radiocarbon dating for the past ~45 ka, indicating that higher log (Fe/Ca) and thus, enhanced rainfall occurs during precession maxima (Fig. 1*D*). Based on this radiocarbon-based phasing, we revisited the age model of GeoB15016 and iteratively performed a fine-tuning of the log (Fe/Ca) record to precession back to 950 ka (Fig. 1 *A*–*C* and *SI Appendix*, Figs. S3 and S4). The resulting age model is consistent with the phasing of the 41-ky obliquity component in our record (*SI Appendix*, Fig. S5).

We interpret the changes in terrigenous input off northern Chile as variations in river runoff caused by winter rain variability, which is related to the strength and location of the Pacific STJ. Today, precipitation along the Pacific margin of South America is nearly entirely controlled by synoptic disturbances embedded within the SWW and zonal wind strength changes are well correlated to rainfall (35). During austral summer, the STJ is weak and the Pacific westerlies are dominated by a midlatitude eddy-driven jet. Consistent with this westerly configuration, subtropical dry climates extend south to ~40°S and high rainfall occurs only over the southernmost South America. During austral winter, the STJ strengthens over Australia and southwestern Pacific and extends eastward. As a result, precipitation extends northward to the southern margin of the Atacama Desert, directly onshore from our core locations. In particular, extreme winter rainfall events over subtropical Chile are caused by warm winter storms from atmospheric river events (35). There is no evidence for significant river discharge originating from summer rainfall at the southern boundary of the Atacama Desert (32).

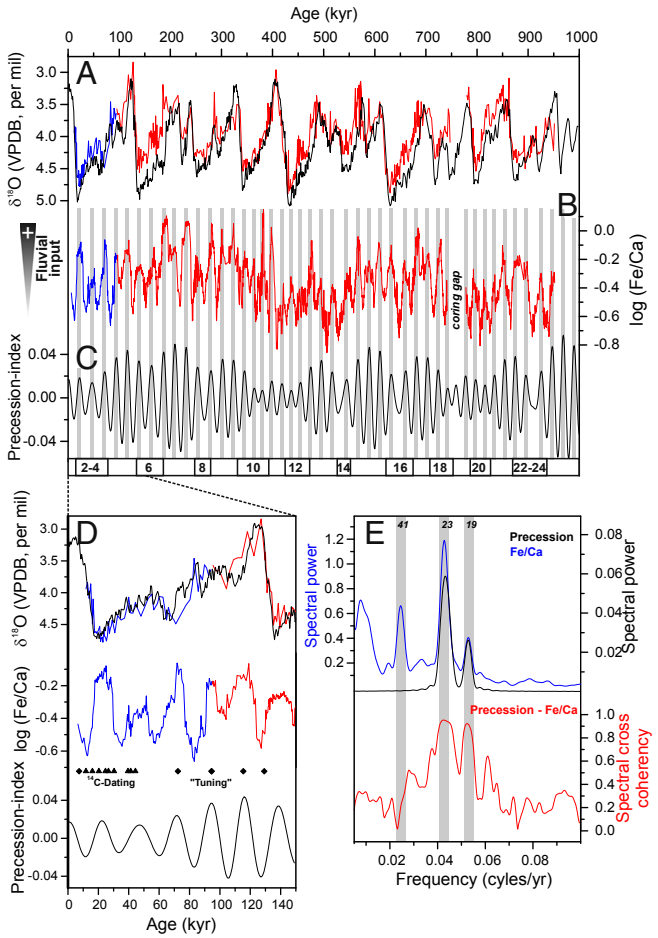

Fig. 1. Sedimentological data, stratigraphy, and spectral pattern. (*A*) Benthic foraminifera oxygen isotope data (blue: core GeoB3375-1, red: GeoB15016) versus LR04 stack (59). (*B*) log (Fe/Ca) record documenting changes in fluvial sediment input (*SI Appendix*, Fig. S2). (*C*) Precession index. (*D*) Zoom into last glacial/interglacial cycle with radiocarbon dates and tie points between log (Fe/Ca) and the precession index. Black curve shows intermediate depth Pacific stack (60). (*E*) Cross-spectral analyses (Blackman–Tukey method; 80% confidence interval) precession versus log (Fe/Ca).

There are no continuous continental rainfall records from subtropical Chile south of the Atacama Desert at orbital timescales beyond the last glacial cycle. Discontinuous regional terrestrial records (36, 37) show several more humid intervals over the past ∼200 ka. The best documented is the LGM precession maximum at ∼21 ka, with glaciological evidence for increased precipitation (38) in line with our data, whereas older intervals of paleosoil development only partially correspond to higher log (Fe/Ca) and thus enhanced continental rainfall in our marine record.

In order to mechanistically explain the remarkably strong precessional cycles in our paleoprecipitation records, we evaluated simulations of 2 coupled ocean–atmosphere general circulation models, EC-Earth 2.2 (39) and the Geophysical Fluid Dynamics Laboratory (GFDL) Climate Model 2.1 (40), both orbitally forced by changes to the phase of precession. For each model, simulations were done with the orbital conditions set to either precession maximum or precession minimum, with other boundary conditions being the same (*SI Methods*). Both model simulations show enhanced austral winter precipitation over subtropical Chile during precession maxima (Fig. 2*A* and *SI Appendix*, Fig. S6*A*). The enhanced rainfall is tied to an increase in lower tropospheric water vapor transport from the central tropical South Pacific to subtropical Chile (see vectors in Fig. 2*A*). We attribute the altered moisture transport to a stronger STJ over the western sector of the South Pacific, which in turn allows for increased synoptic disturbances further east (see shading in Fig. 2*B* and *SI Appendix*, Fig. S6*B*). The disturbances "tap" into the warm, moisture-laden air of the tropical Pacific, allowing for the greater export of moisture to subtropical Chile. The subtropical anticyclone over the southeastern Pacific is also weakened and shifted equatorward during precession maxima (*SI Appendix*, Fig. S7). This is consistent with observations that link the occurrence of austral winter precipitation over subtropical arid Chile to a weaker and equatorward-shifted subtropical anticyclone (41). Overall, the simulated changes to the large-scale circulation over the South Pacific all point to a wetter subtropical Chile during precession maxima as compared to precession minima, in agreement with our paleodata.

Both models show a cooling of the eastern equatorial Pacific cold tongue during precession maxima (Fig. 2*C* and *SI Appendix*, Fig. S6*C*), tied to a phase change in the cold tongue annual sea-surface temperature (SST) cycle (42). The key feature relevant to rainfall over subtropical Chile is the zonal SST gradient across the equatorial Pacific. The climatological wintertime Southern Hemisphere storm track has a pronounced zonally asymmetric configuration: as viewed from the South Pole, it resembles a structure that spirals clockwise and poleward starting north of New Zealand, across the South Pacific and Patagonia, peaking over the Indian Ocean, then decays along the Antarctic edge and terminating at the Ross Sea (42). However, Inatsu and Hoskins (43) showed that when the zonal asymmetry in tropical SST is removed, the Southern Hemisphere storm track is pushed poleward and eastward, and the spiral structure is destroyed. The spiral structure in the storm track reflects the presence of the split jet and is conducive to increased synoptic disturbances over the southeastern tropical Pacific (Fig. 2*B* and *SI Appendix*, Fig. S6*B*). This link suggests that increased rainfall over subtropical Chile occurs when the austral winter equatorial zonal SST gradient is large as seen in both model simulations (Fig. 2*C* and *SI Appendix*, Fig. S6*C*). Proxy data-based reconstructions of tropical Pacific SST confirm variability at precessional timescales both in the western Pacific warm pool (44) and in the eastern tropical Pacific (44) (*SI Appendix*, Figs. S8 and S9). However, interpretations of austral winter SST gradient changes are complicated because the warm pool and cold tongue SST records are based on different proxies (Mg/Ca- versus alkenone-based) and reflect opposite seasons (45).

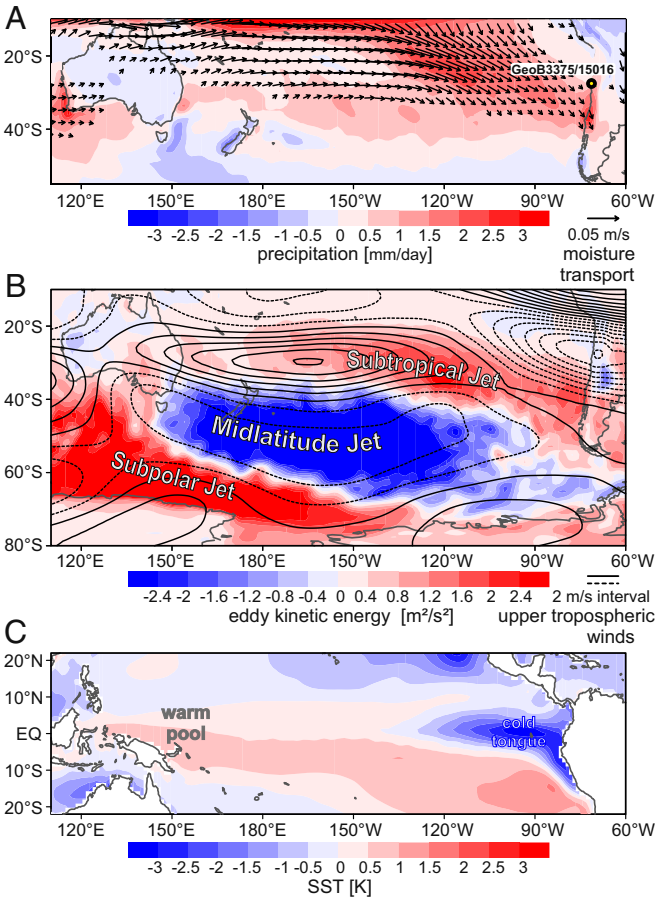

Fig. 2. Simulated June–August climate changes resulting from opposite phases of precession, maximum minus minimum. Shown are the results for EC-Earth; the equivalent figures for GFDL CM2.1 are shown in *SI Appendix*, Fig. S6. June–August averages are shown as those are the months of maximum precipitation over subtropical Chile in the simulation. (*A*) Precipitation (shaded; units are mm/d) and 850-mb moisture transport (wind speed and direction qv; reference vector is 0.05 m/s). For clarity, vectors with zonal components less than +0.005 m/s are not shown. The circle marks the location of the sediment cores. The figure shows increased moisture transport from the central tropical Pacific to subtropical Chile, leading to increases in rainfall there. (*B*) Upper tropospheric winds (200 mb; contour interval 2 m/s) and 2–8-d filtered eddy kinetic energy (shaded; units are m^2/s^2). The latter field is a measure of synoptic eddy activity or "storminess;" we highlight the increased storminess over the southeastern tropical Pacific, coincident with the increased moisture transport and rainfall to subtropical Chile, (*C*) SST (shaded; units are K). In *B*, the approximate locations of the climatological subtropical, midlatitude, and subpolar jets are labeled; and in *C*, the locations of the climatological cold tongue and warm pool regions.

Orbital-Scale Variability of the SWW

On a global scale, we do not find conclusive proxy evidence for orbital-scale SWW variations in other Southern Hemisphere sectors. Sediment records from the northern margin of the SWW, linked to changes in the SWW south of Africa, suggest northward-extended westerlies during glacials (beyond precessional timescales), which increased winter rain and fluvial supply in SW Africa (25). An 800-ka SST record from the Agulhas Current off southeast Africa (Fig. 3*E*) indicates that these changes were accompanied by northward shifts of the subtropical front (22), which would be consistent with a strengthening of the STJ in the Western Indian Ocean–Atlantic sector. Spectral analysis of the SST record does not reveal significant variability on precessional timescales and is instead dominated by 100-ka glacial-interglacial cycles (*SI Appendix*, Fig. S10). Some evidence exists for processional changes

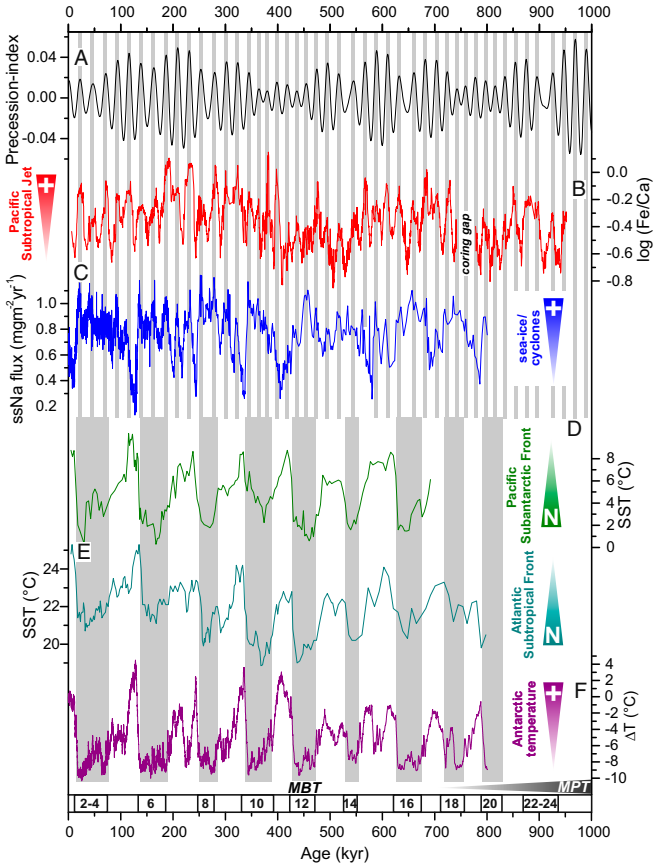

Fig. 3. Comparison to other SWW-related records. (*A*) Precession index. (*B*) log (Fe/Ca) record as a proxy for changes in the strength of the Pacific STJ. (*C*) ssNa flux record of the EDC ice core (53, 61). (*D*) Southeast Pacific SST changes (PS75/34) indicating shifts in the subantarctic front and the midlatitude SWW (23). (*E*) SST south of SE Africa (MD96/2077) documenting variations in the subtropical front in the western Indian Ocean/Atlantic (22). (*F*) Temperature record of the EDC ice core (62). Gray bars across *A*–*C* mark precession maxima (reduced austral winter and higher austral summer insolation); Gray bars across *D*–*F* mark glacial marine isotope stages numbered below; MBT = Mid-Brunhes Event; MPT = Middle Pleistocene Transition.

of winter rain in adjacent South Africa based on speleothem and pollen records, but the precession cycles are only identified back to ~300 ka and are not persistent through time, due to overlapping summer and winter rainfall changes at these locations (46, 47). Taken together, these proxy results are consistent with the reconstructed and modeled strength of the STJ, which is enhanced during precession maxima over the South Pacific, but weaker over the Atlantic and Western Indian Ocean sectors (*SI Appendix*, Fig. S9). This essentially increases the zonal asymmetry in the subtropical westerlies, which are generally stronger in the South Pacific sector and weaker in the other basins.

Within the context of modern climatology, we infer that this unique Pacific pattern is related to a long-term (i.e., precessional) modulation of the South Pacific split jet, not present in the other SWW sectors. A number of South Pacific paleoclimate records over the last glacial termination have been related to a split-jet response to millennial-scale North Atlantic cooling intervals (11). This interhemispheric teleconnection is thought to operate through a southward shift of the Intertropical Convergence Zone and a weakening of the Asian monsoon induced by North Atlantic cooling and is similar to the previously suggested interhemispheric processes across glacial terminations (4, 16, 48). The occurrence of precessional cycles in the Pacific STJ supports the concept of a strong role of orbital precession in modulating interhemispheric temperature gradients and latitudinal shifts of the SWW (48).

Traditionally, precessional forcing has been primarily related to summer insolation changes, particularly as it affects changes in monsoonal rainfall in both hemispheres (49). During precession maxima, higher austral summer insolation enhanced the South American summer monsoon (50), whereas our proxy-reconstructed and modeled enhancement of the STJ during precession maxima occurred in austral winter, the opposite season. At the same precession phase, boreal summer insolation and Northern Hemisphere summer monsoons were reduced (49). This pattern either documents a dynamical link of the Pacific STJ to changes in the monsoonal systems, potentially involving the Northern Hemisphere westerly jet (51), or an independent response of both to precessional forcing.

Our 2 model simulations suggest a close link of a strengthened STJ to enhanced austral winter zonal SST gradients in the equatorial Pacific (Fig. 2*C* and *SI Appendix*, Fig. S6*C*). This link indicates a strong tropical forcing on the extratropical westerlies, similar to what is seen in the response to El Niño-Southern Oscillation variation (1). The strong meridional teleconnections in the South Pacific region appear to be reduced during austral summer. An ~700-ka alkenone SST record from the subantarctic SE Pacific has been interpreted in terms of northward-shifting Southern Ocean fronts and the SWW during glacials and more southward locations during interglacials (23) (PS75/34; Fig. 3*D*). Alkenones are strongly biased toward austral summer at high latitudes (23, 52) and the SST record does not reveal substantial precessional cyclicity. Instead, the SST record is dominated by ~41- and ~100-ka cycles, similar to the subtropical front record from the western Indian Ocean/Atlantic sector (*SI Appendix*, Fig. S10*A*).

Connection to High-Latitude Atmosphere–Ocean Processes

Orbital-scale variability in many paleoclimate records from high- and midlatitudes is primarily dominated by ~41-ka (obliquity) and ~100-ka (eccentricity) cycles. In contrast, our austral winter STJ records show pronounced precessional cycles and only reduced spectral power at the obliquity and eccentricity orbital band (*SI Appendix*, Fig. S10), the latter most likely reflecting more global climate changes in response to glacial/interglacial cycles. Consistent with modern interannual variations (35) at precessional timescales, our model results indicate out-of-phase variations of the STJ/subpolar jet (stronger during precession maxima) compared to the intercalated midlatitude branch (weaker during precession maxima) of the upper-tropospheric Pacific SWW during austral winter (Fig. 2*B*). Austral winter changes of atmosphere–ocean processes in the Southern Ocean are not well constrained as paleoproxy data are rare. One exception is changes in sea-salt sodium (ssNa) flux recorded in the ~800-ka EPICA Dome C (EDC) ice-core record (53) (Fig. 3*C*), which have been interpreted in terms of large-scale winter sea-ice extent around Antarctica. Spectral analyses document strong power in the precessional 19/23-ka bands compared to the dominating 100-ka cyclicity in the ssNa record (*SI Appendix*, Fig. S10*A*). These spectral characteristics are different from the local Antarctic temperature record based on the same ice core, which primarily shows ~41- and ~100-ka cycles (Fig. 3*F* and *SI Appendix*, Fig. S10*A*). The occurrence of strong precessional cycles in both Antarctic ssNa and our Pacific SWW records suggests a mechanistic link. Overall, the ssNa flux is higher during precession maxima (including the LGM) coinciding with our stronger simulated STJ/subpolar jet and weaker midlatitude jet. However, ssNa fluxes at orbital timescales in the EDC ice core may not only reflect large-scale changes in the extent of sea ice around Antarctica (54). Alternatively, the supply of sea spray might be controlled by changes in midlatitude and/or subpolar cyclogenesis (55). Cyclonic activity along the sea-ice edge

might act as an effective source for sea spray being uplifted to sufficient altitudes for transport to the high-altitude EDC site (56).

Conclusions

Our combined proxy and climate model results document substantial orbital-scale changes in the South Pacific jet stream configuration over the past 1 Ma, primarily paced by precession. The amplitudes of ∼41- and ∼100-ka cycles, often dominating midlatitude and high-latitude orbital variability, are strongly reduced in our records, suggesting prevailing tropical forcing of the South Pacific westerlies during austral winter. For precession maxima (including the LGM at ∼21 ka), we plausibly infer a stronger South Pacific split jet with enhanced STJ and subpolar jets and weaker midlatitude jet during austral winter (*SI Appendix*, Fig. S11). Conversely, we derive reduced STJ and subpolar jets, and enhanced midlatitude jet, for precession minima. The presence of precessional cycles in the Pacific SWW, and lack thereof in other basins, indicate that orbital-scale changes of the SWW were not zonally homogeneous across the Southern Hemisphere, in contrast to the hemispherewide shifts of the SWW suggested for glacial terminations and on millennial timescales (4, 16, 48).

The unique response of the Pacific sector of the SWW to precessional forcing in the tropics, shown by model and proxy results, strongly supports a tropical Pacific driver at orbital timescales in the South Pacific, at least during austral winter. The atmosphere–ocean pattern during precession maxima including the LGM are similar to modern La Niña-like states. During austral summer, the available proxy data support zonally more symmetric shifts of the SWW paced by ∼41- and ∼100-ka cycles. These patterns resemble modern changes in the Southern Annular Mode (57). Our reconstructed austral winter precessional cycles appear to persist across Late and Middle Pleistocene ∼100-ka-paced glacial–interglacial cycles and major climate reorganizations such as the Mid-Brunhes Event and the Middle Pleistocene Transition. Austral winter SWW changes along the Southern Ocean ACC might have affected winter-controlled changes in the mixed layer depth, the formation of intermediate water, and the built-up of sea ice around Antarctica (20) during past climates. Our results support recent model simulations, suggesting that precessional forcing of wind stress across the Southern Ocean may play an important role in atmosphere–ocean changes that impact atmospheric CO_2 concentrations (58). The strong meridional teleconnections in the Pacific SWW might therefore have affected global overturning circulation and the storage of atmospheric CO_2 in the deep Pacific Ocean. Furthermore, they might have influenced the exchange of heat, salt, and nutrients between ocean basins, as well as between high and low latitudes.

Methods

We updated the published age models of the sediment records (*SI Methods*). High-resolution major element records were obtained with an X-ray fluorescence core scanner (XRF) and quantification using inductively coupled plasma optical emission spectrometry. Grain-size distributions were obtained on a Coulter laser-granulometer (LS-200). We used Blackman–Tukey spectral analyses to derive the relative power of the major cycles in the Milankovitch band. We performed model simulations with EC-Earth 2.2 (39) fully coupled ocean–atmosphere general circulation model as well as with the GFDL Climate Model version 2.1 (GFDL CM2.1) (40).

Data Availability Statement. All data discussed in the paper have been made available to readers.

ACKNOWLEDGMENTS. We thank the scientific party, captain, and crew of R/V Sonne cruise SO-211. We thank T. Westerhold and V. Lukies for assistance during the XRF scanning. We thank A. J. Broccoli, M. P. Erb, and B. Raney for providing the GFDL model output used in this study. C. Lange, T. Ronge, T. Westerhold, and R. Tiedemann provided comments and suggestions that improved the paper. We acknowledge financial support for this work through the German Research Ministry, which funded this cruise within the project "Paläoumweltgeschichte des Peru-Chile Stroms und des angrenzenden Chile über die letzten Glazial-Interglazial-Zyklen (SO-211)" and supported this project through Palmod Project PalMod 3.2 TP4 (FKZ01LP1510D). Further support was provided by the AWI Helmholtz-Zentrum für Polar- und Meeresforschung and the MARUM–Center for Marine Environmental Sciences. J.C.H.C. acknowledges support from US National Science Foundation Grant 1537496. The computing budget for the EC-Earth simulations was provided by Utrecht University in a "Focus en Massa" grant, with support from the Faculty of Geoscience as well as the Royal Netherlands Meteorological Institute.

1. X. J. Yuan, M. R. Kaplan, M. A. Cane, The interconnected global climate system-A review of tropical-polar teleconnections. *J. Clim.* **31**, 5765–5792 (2018).
2. A. J. Watson, G. K. Vallis, M. Nikurashin, Southern Ocean buoyancy forcing of ocean ventilation and glacial atmospheric CO2. *Nat. Geosci.* **8**, 861–864 (2015).
3. L. C. Allison, H. L. Johnson, D. P. Marshall, D. R. Munday, Where do winds drive the Antarctic Circumpolar Current? *Geophys. Res. Lett.* **37**, L12605 (2010).
4. R. F. Anderson *et al*., Wind-driven upwelling in the Southern Ocean and the deglacial rise in atmospheric CO2. *Science* **323**, 1443–1448 (2009).
5. L. Menviel *et al*., Southern Hemisphere westerlies as a driver of the early deglacial atmospheric CO_2 rise. *Nat. Commun.* **9**, 2503 (2018).
6. F. Lamy *et al*., Holocene changes in the position and intensity of the southern westerly wind belt. *Nat. Geosci.* **3**, 695–699 (2010).
7. K. M. Saunders *et al*., Holocene dynamics of the Southern Hemisphere westerly winds and possible links to CO2 outgassing. *Nat. Geosci.* **11**, 650–655 (2018).
8. A. E. Shevenell, A. E. Ingalls, E. W. Domack, C. Kelly, Holocene Southern Ocean surface temperature variability west of the Antarctic Peninsula. *Nature* **470**, 250–254 (2011).
9. C. D. Hillenbrand *et al*., West Antarctic Ice Sheet retreat driven by Holocene warm water incursions. *Nature* **547**, 43–48 (2017).
10. T. M. Bals-Elsholz *et al*., The wintertime Southern Hemisphere split jet: Structure, variability, and evolution. *J. Clim.* **14**, 4191–4215 (2001).
11. J. C. H. Chiang, S. Y. Lee, A. E. Putnam, X. F. Wang, South Pacific Split Jet, ITCZ shifts, and atmospheric North-South linkages during abrupt climate changes of the last glacial period. *Earth Planet. Sci. Lett.* **406**, 233–246 (2014).
12. S. N. Chenoli, M. Y. A. Mazuki, J. Turner, A. Abu Samah, Historical and projected changes in the Southern Hemisphere Sub-tropical Jet during winter from the CMIP5 models. *Clim. Dyn.* **48**, 661–681 (2017).
13. L. B. Hande, S. T. Siems, M. J. Manton, Observed trends in wind speed over the Southern Ocean. *Geophys. Res. Lett.* **39**, L11802 (2012).
14. C. J. Heusser, Southern westerlies during the last glacial maximum. *Quat. Res.* **31**, 423–425 (1989).
15. K. E. Kohfeld *et al*., Southern Hemisphere westerly wind changes during the last glacial maximum: Paleo-data synthesis. *Quat. Sci. Rev.* **68**, 76–95 (2013).
16. G. H. Denton *et al*., The last glacial termination. *Science* **328**, 1652–1656 (2010).
17. S. Y. Lee, J. C. H. Chiang, K. Matsumoto, K. S. Tokos, Southern Ocean wind response to North Atlantic cooling and the rise in atmospheric CO(2): Modeling perspective and paleoceanographic implications. *Paleoceanography* **26**, PA1214 (2011).
18. B. R. Markle *et al*., Global atmospheric teleconnections during Dansgaard-Oeschger events. *Nat. Geosci.* **10**, 36–40 (2017).
19. H. C. Bostock, B. W. Hayward, H. L. Neil, A. T. Sabaa, G. H. Scott, Changes in the position of the Subtropical Front south of New Zealand since the last glacial period. *Paleoceanography* **30**, 824–844 (2015).
20. J. C. H. Chiang, K. S. Tokos, S. Y. Lee, K. Matsumoto, Contrasting impacts of the South Pacific Split Jet and the Southern Annular Mode Modulation on Southern Ocean circulation and biogeochemistry. *Palaeogeogr. Palaeoclimatol.***33**, 2–20 (2018).
21. X. J. Yuan, ENSO-related impacts on Antarctic sea ice: A synthesis of phenomenon and mechanisms. *Antarct. Sci.* **16**, 415–425 (2004).
22. E. Bard, R. E. M. Rickaby, Migration of the subtropical front as a modulator of glacial climate. *Nature* **460**, 380–383 (2009).
23. S. L. Ho *et al*., Sea surface temperature variability in the Pacific sector of the Southern Ocean over the past 700 kyr. *Paleoceanography* **27**, PA4202 (2012).
24. F. Lamy *et al*., Increased dust deposition in the Pacific Southern Ocean during glacial periods. *Science* **343**, 403–407 (2014).
25. J.-B. W. Stuut *et al*., A 300-kyr record of aridity and wind strength in southwestern Africa: Inferences from grain-size distributions of sediments on Walvis Ridge, SE Atlantic. *Mar. Geol.* **180**, 221–233 (2002).
26. F. Lamy, D. Hebbeln, G. Wefer, Late quaternary precessional cycles of terrigenous sediment input off the Norte Chico, Chile (27.5 degrees S) and palaeoclimatic implications. *Palaeogeogr. Palaeoclimatol. Palaeoecol.* **141**, 233–251 (1998).
27. G. Martinez-Mendez *et al*., Changes in the advection of Antarctic intermediate water to the northern Chilean coast during the last 970 kyr. *Paleoceanography* **28**, 607–618 (2013).
28. G. J. Weltje, R. Tjallingii, Calibration of XRF core scanners for quantitative geochemical logging of sediment cores: Theory and application. *Earth Planet. Sci. Lett.* **274**, 423–438 (2008).
29. F. Lamy, J. Klump, D. Hebbeln, G. Wefer, Late Quaternary rapid climate change in northern Chile. *Terra Nova* **12**, 8–13 (2000).

30. F. Lamy, D. Hebbeln, G. Wefer, Terrigenous sediment supply along the Chilean continental margin: Modern regional patterns of texture and composition. *Geol. Rundsch.* **87**, 477–494 (1998).
31. J. B. W. Stuut, S. Kasten, F. Lamy, D. Hebbeln, Sources and modes of terrigenous sediment input to the Chilean continental slope. *Quat. Int.* **161**, 67–76 (2007).
32. V. Favier, M. Falvey, A. Rabatel, E. Praderio, D. Lopez, Interpreting discrepancies between discharge and precipitation in high-altitude area of Chile's Norte Chico region (26-32 degrees S). *Water Resour. Res.* **45**, W02424 (2009).
33. J. Houston, Variability of precipitation in the Atacama desert: Its causes and hydrological impact. *Int. J. Climatol.* **26**, 2181–2198 (2006).
34. L. Dezileau *et al*., Iron control of past productivity in the coastal upwelling system off the Atacama Desert, Chile. *Paleoceanography* **19**, PA3012 (2004).
35. R. Garreaud, P. Lopez, M. Minvielle, M. Rojas, Large-scale control on the patagonian climate. *J. Clim.* **26**, 215–230 (2013).
36. H. Veit, F. Preusser, M. Trauerstein, The Southern Westerlies in Central Chile during the two last glacial cycles as documented by coastal aeolian sand deposits and intercalating palaeosols. *Catena* **134**, 30–40 (2015).
37. J. Zech, C. Terrizzano, E. Garcia-Morabito, H. Veit, R. Zech, Timing and extent of late Pleistocence glaciation in the arid central Andes of Argentina and CHILE (22 degrees-41 degrees S). *Cuad. Investig. Geogr.* **43**, 697–718 (2017).
38. C. Kull, M. Grosjean, H. Veit, Modeling modern and late Pleistocene glacio-climatological conditions in the north Chilean Andes (29-30 degrees S). *Clim. Change* **52**, 359–381 (2002).
39. J. H. C. Bosmans, S. S. Drijfhout, E. Tuenter, F. J. Hilgen, L. J. Lourens, Response of the North African summer monsoon to precession and obliquity forcings in the EC-Earth GCM. *Clim. Dyn.* **44**, 279–297 (2015).
40. M. P. Erb, C. S. Jackson, A. J. Broccoli, Using single-forcing GCM simulations to reconstruct and interpret quaternary climate change. *J. Clim.* **28**, 9746–9767 (2015).
41. C. Ortega *et al*., Extreme ENSO-driven torrential rainfalls at the southern edge of the Atacama Desert during the Late Holocene and their projection into the 21th century. *Global Planet. Change* **175**, 226–237 (2019).
42. M. P. Erb *et al*., Response of the equatorial pacific seasonal cycle to orbital forcing. *J. Clim.* **28**, 9258–9276 (2015).
43. M. Inatsu, B. J. Hoskins, The zonal asymmetry of the Southern Hemisphere winter storm track. *J. Clim.* **17**, 4882–4892 (2004).
44. K. Tachikawa, A. Timmermann, L. Vidal, C. Sonzogni, O. E. Timm, CO2 radiative forcing and Intertropical Convergence Zone influences on western Pacific warm pool climate over the past 400 ka. *Quat. Sci. Rev.* **86**, 24–34 (2014).
45. A. Timmermann, J. Sachs, O. E. Timm, Assessing divergent SST behavior during the last 21 ka derived from alkenones and G. ruber-Mg/Ca in the equatorial Pacific. *Paleoceanography* **29**, 680–696 (2014).
46. K. Braun *et al*., Late Pleistocene records of speleothem stable isotopic compositions from Pinnacle Point on the South African south coast. *Quat. Res.* **91**, 265–288 (2019).
47. D. H. Urrego, M. F. S. Goni, A. L. Daniau, S. Lechevrel, V. Hanquiez, Increased aridity in southwestern Africa during the warmest periods of the last interglacial. *Clim. Past* **11**, 1417–1431 (2015).
48. J. R. Toggweiler, D. W. Lea, Temperature differences between the hemispheres and ice age climate variability. *Paleoceanography* **25**, PA2212 (2010).
49. M. Mohtadi, M. Prange, S. Steinke, Palaeoclimatic insights into forcing and response of monsoon rainfall. *Nature* **533**, 191–199 (2016).
50. P. A. Baker, S. C. Fritz, Nature and causes of Quaternary climate variation of tropical South America. *Quat. Sci. Rev.* **124**, 31–47 (2015).
51. J. C. H. Chiang *et al*., Role of seasonal transitions and westerly jets in East Asian paleoclimate. *Quat. Sci. Rev.* **108**, 111–129 (2015).
52. F. G. Prahl, J.-F. Rontani, N. Zabeti, S. E. Walinsky, M. A. Sparrow, Systematic pattern in UK'37–Temperature residuals for surface sediments from high latitude and other oceanographic settings. *Geochim. Cosmochim. Acta* **74**, 131–143 (2010).
53. E. W. Wolff *et al*., Southern Ocean sea-ice extent, productivity and iron flux over the past eight glacial cycles. *Nature* **440**, 491–496 (2006).
54. J. G. Levine, X. Yang, A. E. Jones, E. W. Wolff, Sea salt as an ice core proxy for past sea ice extent: A process-based model study. *J. Geophys. Res. Atmos.* **119**, 5737–5756 (2014).
55. B. R. Markle, E. J. Steig, G. H. Roe, G. Winckler, J. R. McConnell, Concomitant variability in high-latitude aerosols, water isotopes and the hydrologic cycle. *Nat. Geosci.* **11**, 853–855 (2018).
56. J. R. Petit, B. Delmonte, A model for large glacial-interglacial climate-induced changes in dust and sea salt concentrations in deep ice cores (central Antarctica): Palaeoclimatic implications and prospects for refining ice core chronologies. *Tellus B Chem. Phys. Meterol.* **61**, 768–790 (2009).
57. N. P. Gillett, D. W. J. Thompson, Simulation of recent southern hemisphere climate change. *Science* **302**, 273–275 (2003).
58. R. L. Rutberg, A. J. Broccoli, Response of high latitude Southern Hemisphere to precessional forcing: Implications for Pleistocene ocean circulation. *Palaeogeogr. Palaeoclimatol.* **34**, 1092–1106 (2019).
59. L. E. Lisiecki, M. E. Raymo, A Pliocene-Pleistocene stack of 57 globally distributed benthic delta O-18 records. *Paleoceanography* **20**, PA1003 (2005).
60. L. E. Lisiecki, J. V. Stern, Regional and global benthic O-18 stacks for the last glacial cycle. *Paleoceanography* **31**, 1368–1394 (2016).
61. E. W. Wolff *et al*., Changes in environment over the last 800,000 years from chemical analysis of the EPICA Dome C ice core. *Quat. Sci. Rev.* **29**, 285–295 (2010).
62. J. Jouzel *et al*., Orbital and millennial Antarctic climate variability over the past 800,000 years. *Science* **317**, 793–796 (2007).